Indian Geotechnical Journal, Vol. 24 (3), 1994

Non Linear Analysis of Rectangular Raft Resting on Soil

by

N.B.S. Rao*

Krishnamoorthy**

Introduction

The load-settlement behavior of foundation resting on soil is generally non -linear.It depends on the stress history, stress path, dilatancy and initial stress conditions. A method which gives a reliable settlement for the applied load taking into consideration all the above factors is required for an appropriate and economical design of foundation. In recent years great interest has been developed in the modelling of the soil behavior and hence a wide range of models are available both for clays and sands, which consider many of the factors mentioned above. The application of these models to practical problems involves much complexity. An attempt is made in this direction by implementing the model suggested by Yin et al (1989) which incorporates non-linearity, stress history, dilatancy and the related phenomenon which produces shear strains due to mean stress changes, to analyse a rectangular raft resting on soil layer of finite depth.

Main Features of the Model Used

The constitutive model presented by Yin et al (1989) is used for the soil in the analysis. The model relates the changes in strains to the corresponding changes in stresses by three modulus functions, a bulk modulus K, a shear modulus G and a modulus J that couples effective mean stress vs shear strain (p', ε_s) and shear stress vs volumetric strain (q', ε_v) behavior. The three modulii can be obtained from the normalized stress strain behavior of soil samples in isotropic consolidation test and (preferably undrained) triaxial compression test.

---

* Professor, Applied Mechanics Deptt., K.R.E.C., Surathkal

** Lecturer, Civil Engineering Deptt., M.I.T., Manipal

The increments of strains corresponding to the increments of stresses are related as,

$$\begin{vmatrix} d\varepsilon_{11} \\ d\varepsilon_{22} \\ d\varepsilon_{33} \\ d\varepsilon_{12} \\ d\varepsilon_{23} \\ d\varepsilon_{31} \end{vmatrix} = \begin{vmatrix} a_1 + 2b_1 & a_2 + b_1 + b_2 & a_2 + b_1 + b_3 & c_1 & c_2 & c_3 \\ a_2 + b_1 + b_2 & a_1 + 2b_2 & a_2 + b_2 + b_3 & c_1 & c_2 & c_3 \\ a_2 + b_1 + b_3 & a_2 + b_2 + b_3 & a_1 + 2b_3 & c_1 & c_2 & c_3 \\ \frac{c_1}{2} & \frac{c_2}{2} & \frac{c_3}{2} & \frac{1}{2G} & 0 & 0 \\ \frac{c_1}{2} & \frac{c_2}{2} & \frac{c_3}{2} & 0 & \frac{1}{2G} & 0 \\ \frac{c_1}{2} & \frac{c_2}{2} & \frac{c_3}{2} & 0 & 0 & \frac{1}{2G} \end{vmatrix} \begin{vmatrix} d\sigma_{11} \\ d\sigma_{22} \\ d\sigma_{33} \\ d\sigma_{12} \\ d\sigma_{23} \\ d\sigma_{31} \end{vmatrix} \quad \ldots\ldots\ldots (1)$$

The determination of the various parameters used in equation (1) is explained in appendix - 1.

Details of the Problem

The constitutive model explained in the previous section is used to represent the soil behavior. The model parameters given by Yin et al (1989)

Table 1.
Curve - fitting parameters

	K-modulus		J-modulus		G-modulus	
	λ/V_i	ε_{vo}	A	n	E	F
Soil 1	0.052	-0.039	1.25	0.65	0.0108	1.83
Soil 2	0.073	-0.003	1.32	0.71	0.0086	2.15
Soil 3	0.029	-0.172	-8.93	1.00	0.0039	0.92

where Soil 1 = Sand - bentonite buffer $I_d > 90$ %
Soil 2 = Sand - bentonite buffer $I_d < 90$ %
Soil 3 = Paris clay.
I_d = Relative density.

have been used for the analysis and are tabulated in table 1. The raft resting on the soil mass and details of the eight noded isoparametric brick element used are shown in Fig. 1. The descretization used is shown in Fig. 2. Figure 3 shows the details of numbering used to represent different elements. The elements are numbered in vertical rows starting from the centre of the raft and increasing towards x-direction. There are six rows of eight noded elements. The various rows considered are numbered in Fig. 2. Here, L is the length, B the width and t the thickness of the raft resting on the surface of the soil layer of finite thickness H bounded by a horizontal ground surface at top and a rough rigid base at the bottom. The horizontal displacement of soil layer is restrained at a distance of 5b or 5l from the edge of the raft, where b = B/2 and l = L/2.The depth of the soil layer H is taken as equal to two times the width of the raft.

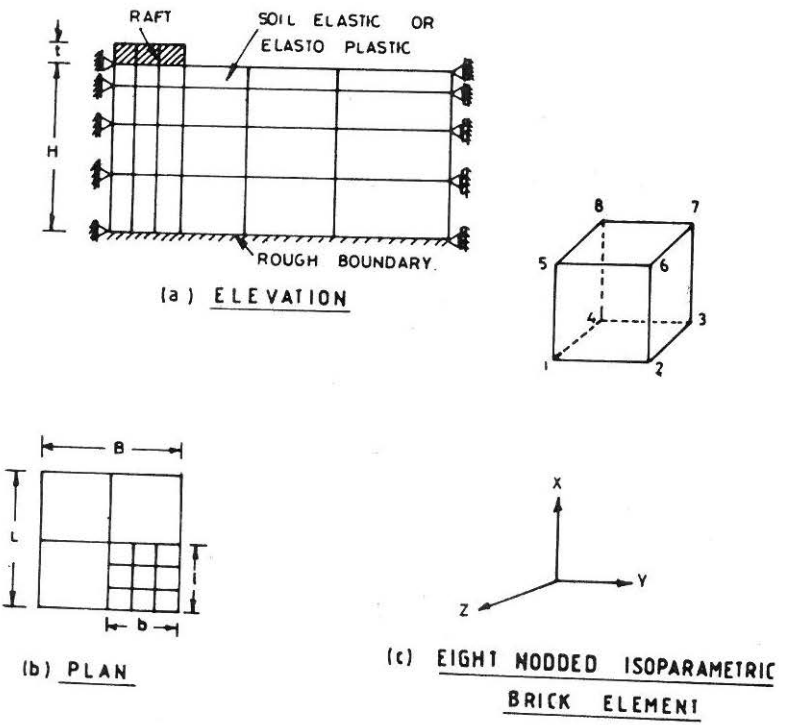

(a) Descritization of soil raft system

(b) Plan of raft

(c) Details of elements used

FIGURE 1 Raft Resting On Soil Mass

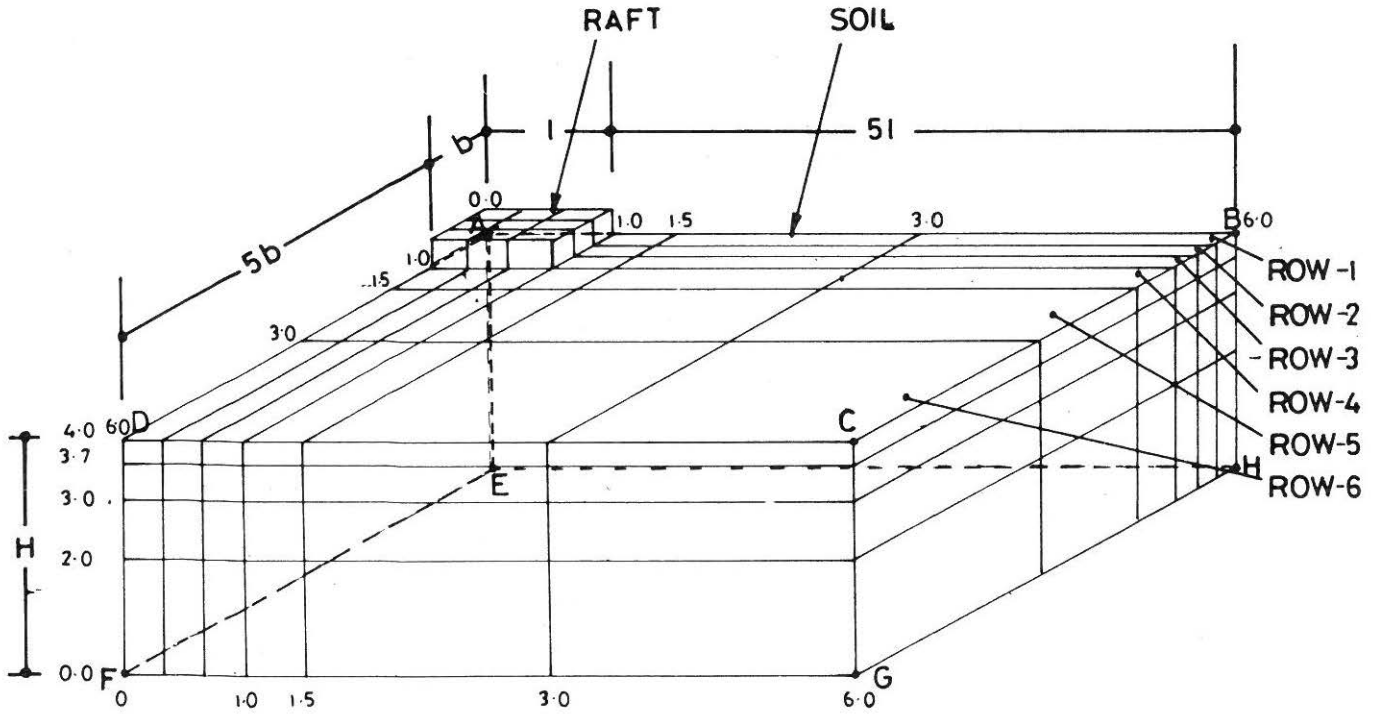

FIGURE 2 Finite Element Idealization Of Raft And Solil

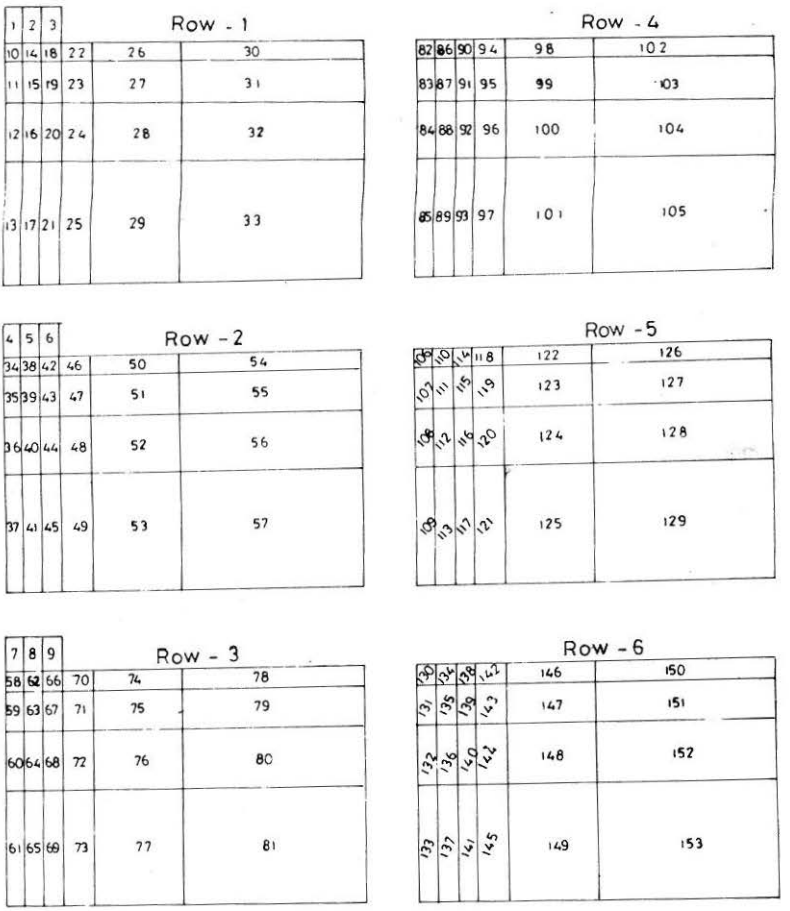

FIGURE 3 Details of Element Numbers

The various boundary conditions applied are as follows

The displacement in the X-direction = 0 along the face DCGF

The displacement in the Y-direction = 0 along the face BCGH

The displacement in the X-direction = 0 along the face ABHE

The displacement in the Y-direction = 0 along the face AEFD

The displacement in the X, Y, Z direction = 0 along the face EFGH

The soil-raft system is analysed for three different types of soils, the properties of which as given by Yin et al (1989) are tabulated in table 2.

Table 2.
Soil properties

Soil	Clay fraction (%)	w (%)	I_p (%)	$\sqrt{d}$ (Mg/m³)	ϕ (deg)	V_i
Soil 1.	50	250	200	1.50	13	1.76
Soil 2.	50	250	200	1.67	14	1.61
Soil 3.	60	64	33	1.59	22	1.75

where V_i = Initial specific volume.
w = Water content.
I_p = Plasticity Index.
$\sqrt{d}$ = Unit weight of soil.
ϕ = Angle of Internal friction.

Numerical Procedure

The raft is considered as elastic and the elastic constants corresponding to reinforced concrete are used in the analysis. Since the model used for the analysis of soil is in the incremental form, an incremental solution technique has been used. A mixed procedure consisting of incremental and iterative scheme as suggested by Desai and Abel (1972) is found to be suitable and hence this method is adapted in the numerical procedure.Optimum values of Elastic constants E and μ for the elastic continuum representing the soil are selected and a small increment of load (1/10 of load corresponding to preconsolidation pressure) is applied. The corresponding increments of stesses ($d\varepsilon'_{11}$, $d\varepsilon'_{22}$, $d\varepsilon'_{33}$, $d\varepsilon'_{12}$, $d\varepsilon'_{23}$, $d\varepsilon'_{31}$)and strains($d\varepsilon_{11}$, $d\varepsilon_{22}$, $d\varepsilon_{33}$, $d\varepsilon_{12}$, $d\varepsilon_{23}$, $d\varepsilon_{31}$) are computed by displacement Finite Element Method.

The corresponding values of increments of volumetric strains ($d\varepsilon_{ve}$) and shear strains ($d\varepsilon_{se}$) are calculated by the following equation,

$$d\varepsilon_{ve} = \left(d\varepsilon_{11} + d\varepsilon_{22} + d\varepsilon_{33}\right) \tag{2}$$

$$d\varepsilon_{se}^{2} = 2/9\left[\begin{array}{l}\left(d\varepsilon_{11} - d\varepsilon_{22}\right)^2 + \left(d\varepsilon_{22} - d\varepsilon_{33}\right)^2 \\ \quad + \left(d\varepsilon_{33} - d\varepsilon_{11}\right)^2 + 3/2\left(d\varepsilon_{12}^{2} + d\varepsilon_{23}^{2} + d\varepsilon_{31}^{2}\right)\end{array}\right] \tag{3}$$

The increments of effective mean stress (dp') and deviator stress (shear

stress) (dq) are then computed from the equations,

$$dp' = \left(d\sigma'_{11} + d\sigma'_{22} + d\sigma'_{33}\right)/3 \tag{4}$$

$$dq = \frac{1}{\sqrt{2}}\left[\begin{array}{l}\left(d\sigma_{11} - d\sigma_{22}\right)^2 + \left(d\sigma_{22} - d\sigma_{33}\right)^2 \\ \quad + \left(d\sigma_{33} - d\sigma_{11}\right)^2 + 6\left(d\sigma_{12}^{\ 2} + d\sigma_{23}^{\ 2} + d\sigma_{31}^{\ 2}\right)\end{array}\right]^{1/2} \tag{5}$$

The values of dp′ and dq obtained from equation (4) and equation (5) are added to the current step values of p′ and q to get new values of p′ and q for each increment of load. Initially $p' = P'_{cons}$ and $q = 0$ are taken for the analysis.

The modulus K, G and J are then calculated using p′ and q corresponding to previous stress level and the strain increments for load increment are obtained by using the constitutive equation (1).

The corresponding volumetric strain ($d\varepsilon_{vm}$) and shear strain ($d\varepsilon_{sm}$) increments are calculated from equation

$$d\varepsilon_{vm} = \left(d\varepsilon_{11} + d\varepsilon_{22} + d\varepsilon_{33}\right) \tag{6}$$

$$d\varepsilon_{sm}^{\ 2} = 2/9\left[\begin{array}{l}\left(d\varepsilon_{11} - d\varepsilon_{22}\right)^2 + \left(d\varepsilon_{22} - d\varepsilon_{33}\right)^2 \\ \quad + \left(d\varepsilon_{33} - d\varepsilon_{11}\right)^2 + 3/2\left(d\varepsilon_{12}^{\ 2} + d\varepsilon_{23}^{\ 2} + d\varepsilon_{31}^{\ 2}\right)\end{array}\right] \tag{7}$$

Where $d\varepsilon_{11}$, $d\varepsilon_{22}$, $d\varepsilon_{33}$, $d\varepsilon_{12}$, $d\varepsilon_{23}$, $d\varepsilon_{31}$ are the incremental strain obtained for the model by using the constitutive equation (1). The volumetric strain ($d\varepsilon_{vm}$) and shear strain ($d\varepsilon_{sm}$) obtained by the model is compared with the volumetric strain ($d\varepsilon_{ve}$) and shear strain ($d\varepsilon_{se}$) obtained for the elastic continuum by the displacement Finite Element Analysis. If they do not match to the specified accuracy (generally 0.000001), the elastic continuum with constant E and μ is analysed several times, subjected to different self equilibrating nodal forces. The initial strain used in computing the nodal forces is the difference between the strains computed by the two methods or a fraction of the difference.

Once the induced strains due to the applied load increments are adjusted by the above procedure, the subsequent load increment is applied and the process is continued till the required number of load increments are applied.

Discussion of the Results

Figure 4 shows the load-deformation behavior for three different types of soils. The load-deformation behavior is non-linear from the beginning and shows the yield point clearly for all the three types of soils.

As the load is applied in increments, the stresses in the element change. The successive states of stresses for each element for each increment of load is shown in Fig. 5 as a stress path.It was observed from the stresses computed that neglecting the small variations, the stress paths followed by various elements can be grouped into four distinct stress paths. The element numbers and the corresponding stress paths are tabulated in table 3.

The elements situated immediately below the raft and near the ground surface follow path 1. This path lies between the conventional A and E paths as indicated in Fig. 5. These elements are subjected to large changes in effective mean stresses and shear stresses for each increment of load.

The elements situated considerably below the raft and elements situated immediately adjacent to the raft from top to bottom will follow path 2. This path lies between the conventional A and B paths. The elements on these

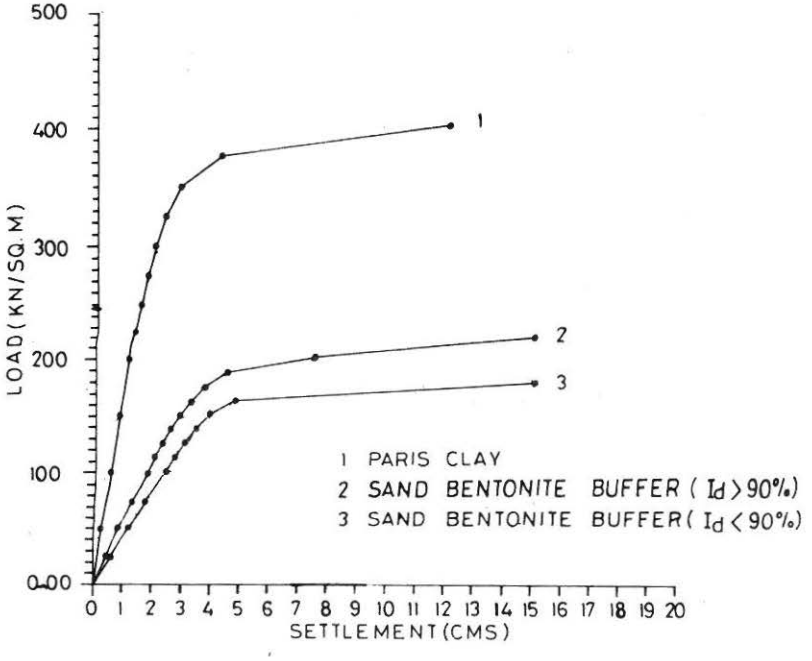

FIGURE 4 Load - Deformation Behaviour Using Three Types Of Soils As Obtained By Present Analysis

paths are subjected to higher changes in shear stresses compared to the changes in effective mean stresses.

The elements situated away from the raft and near the ground surface will follow path 3. This path closely follows the conventional C path. The elements on these paths are subjected to small changes in shear stresses and effective mean stresses. For each increment of load, the effective mean stress on these elements decreases as the load increases.

The elements situated near the boundaries of the soil considered from ground surface to the bottom of the soil will follow path 4. This path closely follows the conventional path B. These elements are subjected to small changes in shear stresses without much change in effective mean stress and hence the path is close to the constant mean stress path.

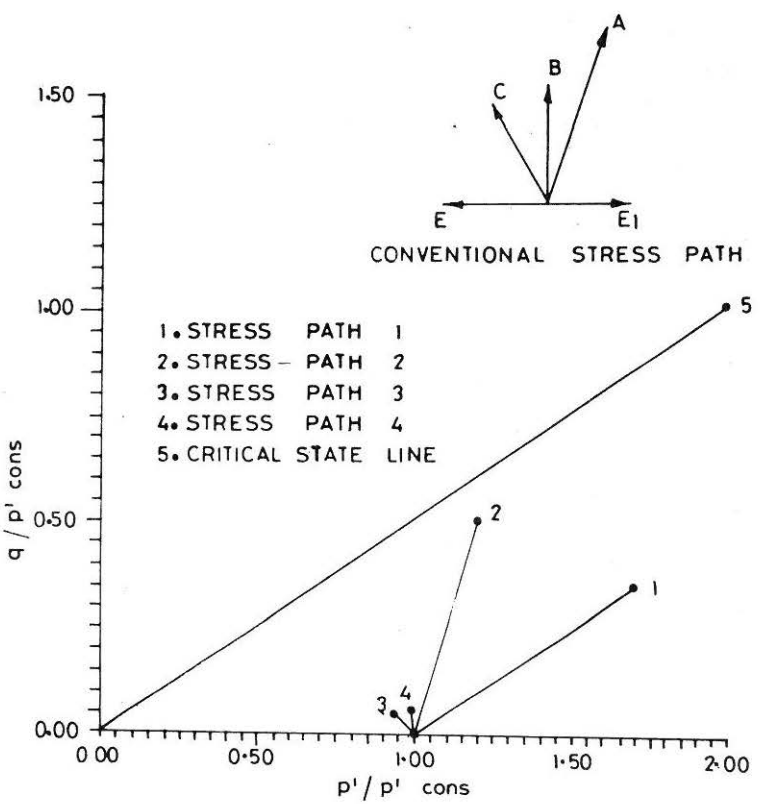

FIGURE 5(a) Stress Paths Followed By Various Elements For Sand Bentonite Buffer (I_d > 90%)

Table 3.
Stress Path Followed by Various Elements

Path	Element Numbers
1	10, 14, 18, 34, 38, 42, 58, 62, 66
2	11, 12, 13, 15, 16, 17, 19, 20, 21, 22, 23, 24, 25, 27, 28, 29, 35, 36, 37, 39, 40, 41, 43, 44, 45, 46, 47, 48, 49, 51, 52, 53, 59, 60, 61, 63, 64, 65, 67-73, 75-77, 82-97, 99-101, 107-109, 111-113, 115-117, 119-121, 123-125
3	26, 50, 74, 98, 106, 110, 114, 118, 122
4	30-33, 54-57, 78-81, 102-105, 126-153

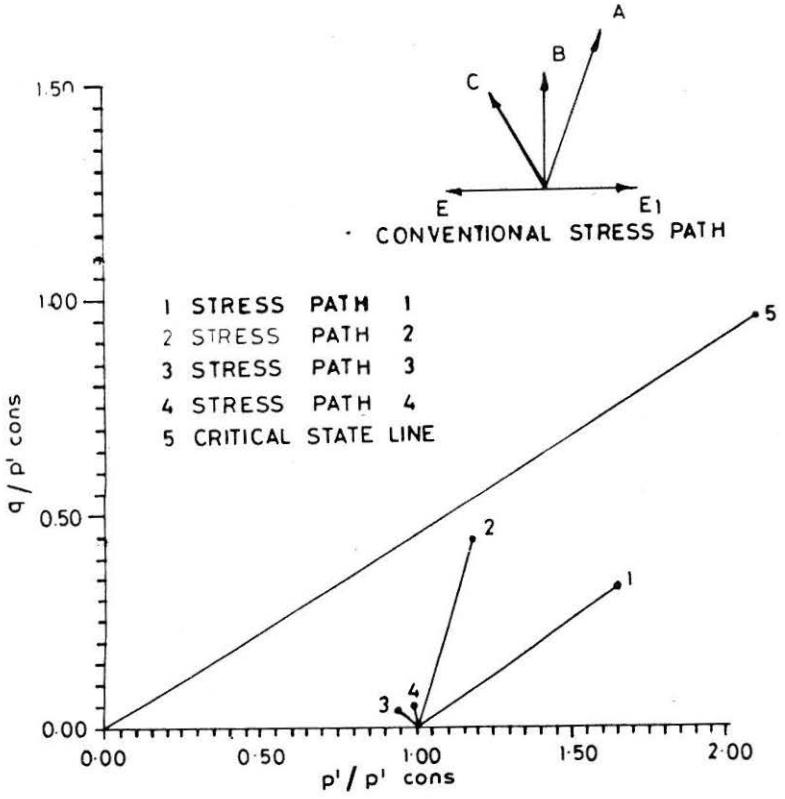

FIGURE 5(b) Stress Paths Followed By Various Elements For Sand Bentonite Buffer (I_d < 90%)

The critical state line as suggested by Atkinson and Bransby (1978) is also plotted on q/P'_{cons} vs P'/P'_{cons} relationship as shown in Fig. 5. The stress paths followed by all the elements for all the three types of soil lie below the critical state line. The elements for the loads considered start yielding as the stress path approaches the critical state line.

Fig. 6 shows the relationship between load vs volumetric strain for four different stress paths followed by the elements. As per the sign conventions adopted, the positive volumetric strain implies a decrease in volume and negative volumetric strain implies an increase in the volume of the soil mass.

Figure 6(a) shows the relationship between load and volumetric strain for sand bentonite buffer (I_d > 90%). For the elements following stress

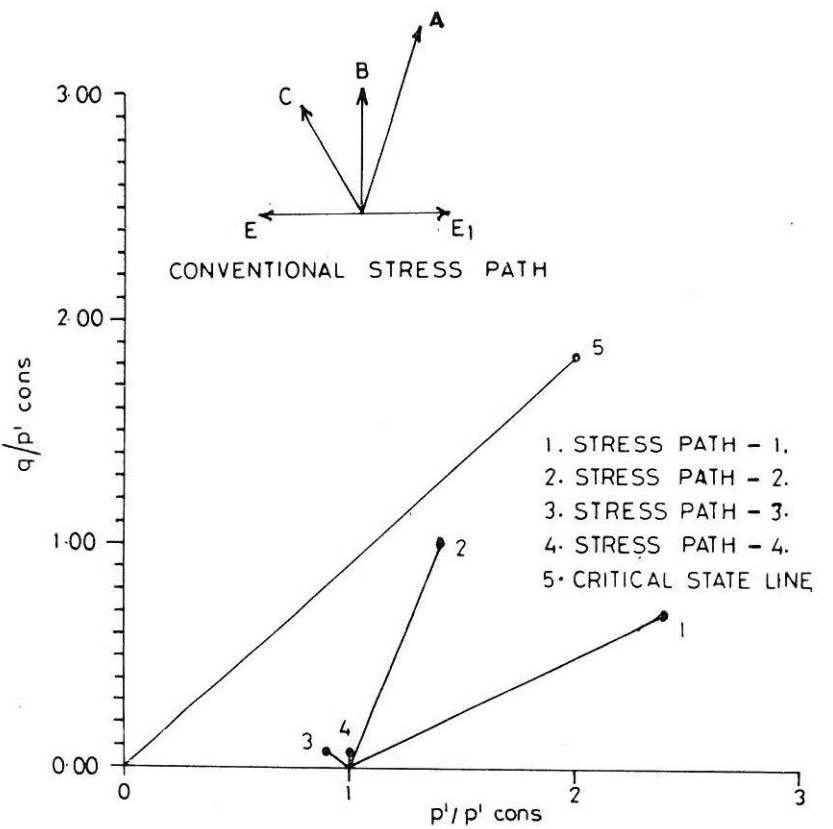

FIGURE 5(c) Stress Paths Followed By Various Elements For Paris Clay

path 1, the volumetric strain is positive and it increases with the load and reaches a maximum value of 3.8% at 215 KN/sq. m load. For the elements following stress path 2 also the volumetric strain is positive and increases with load and reaches a value of 1.5% at 215 KN/sq. m load which is less than that of the elements followig stress path 1. The volumetric strains of the elements following stress path 3 is negative and it increases with the increase in load. The elements following stress path 4 remain almost constant in volume with changes in stresses.

Figure 6(b) shows the load vs volumetric strain relationship for sand bentonite buffer (I_d < 90%). The volumetric strain of the elements following stress path 1 is positive and it increases with the increase in load attaining a maximum volumetric strain of 5%. The volumetric strain for the elements following stress path 2 is also positive and it increases with increase in load and reaches a maximum value of 2.5%. As in the case of sand bentonite buffer (Id > 90 %) the volumetric strain of the elements followig stress path 3 is negative and it increases with load. The elements following stress path 4 remain almost constant in volume with increase in load.

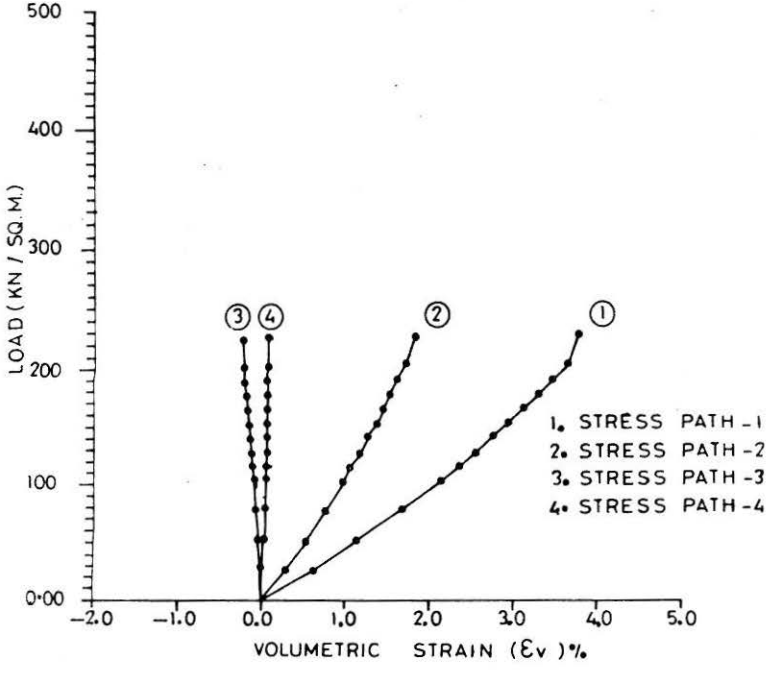

FIGURE 6(a) Load Vs. Volumetric Strain Behaviour For Sand Bentonite Buffer (I_d > 90%)

It is clearly observed from these figures that for a particular stress path the nature of change in volume is same (volume decrease or volume increase) in both types of sand bentonite mixtures. However, the magnitude of change is larger for a soil of lower relative density. Further the sand bentonite buffer (Id > 90 %) exhibits no change in volume for stress path 1 after reaching the stress state close to critical state indicating that the soil element has attained the critical void ratio.

Figure 6(c) shows the load vs volumetric strain relationship for Paris clay. The volumetric strain for elements following stress path 1 and 2 is positive and increases with the load. However the increase in volumetric strain is less compared with the sand bentonite buffer. The elements following stress path 4 will have no change in volume. The volumetric strain for the elements following stress path 3 is negative and it increases considerably with increase in load.

Thus it can be observed from figures 6(a), 6(b) and 6(c) that the volumes of the elements following stress paths 1 and 2 will decrease whereas the volume of the elements following stress path 3 will increase with the

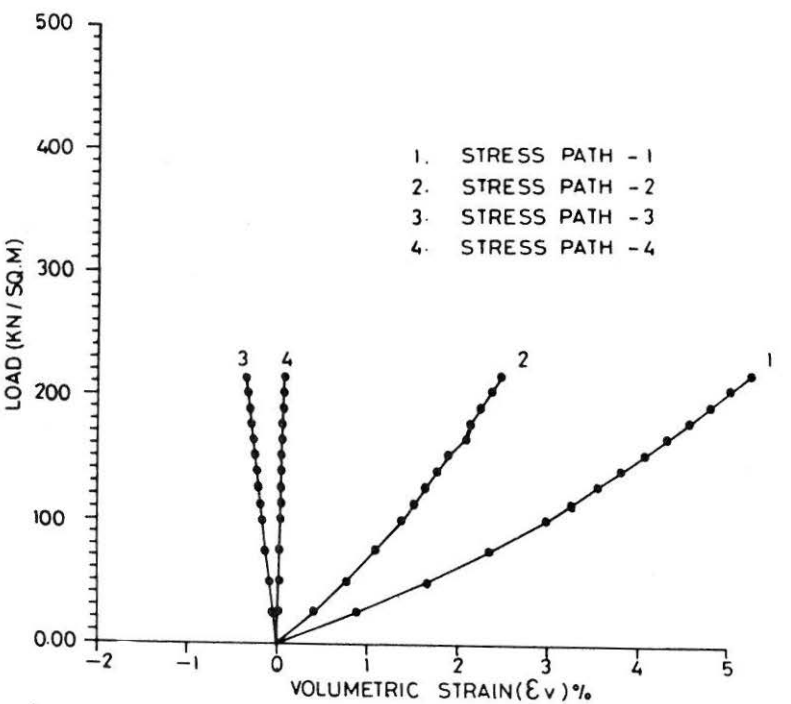

FIGURE 6(b) Load Vs. Volumetric Strain Behaviour For Sand Bentonite Buffer (I_d < 90%)

load. The volume of the elements following stress path 4 remains almost constant with increase in load.

The q/P'_{cons} vs ε_s relationship as obtained by Yin et al (1989) based on undrained triaxial compression test is shown in the Fig. 7. The shape of the load-deformation behavior of the raft obtained by the present analysis shown in Fig. 4 is having the same trend as that of q/P'_{cons} vs ε_s relationship given by Yin et al (1989) for all the three types of soils. Thus the method adopted is capable of incorporating the model and hence can be used to predict the load-deformation behavior of the raft resting on soils. The verification of the applicability of the analysis to field problems is currently in progress by conducting model studies using naturally available soil and results will be reported later.

Conclusions

The non-linear analysis of a rectangular raft resting on soil mass is analysed by implementing the model suggested by Yin et al (1989) to obtain the load-deformation behavior of raft resting on the soil mass. Three

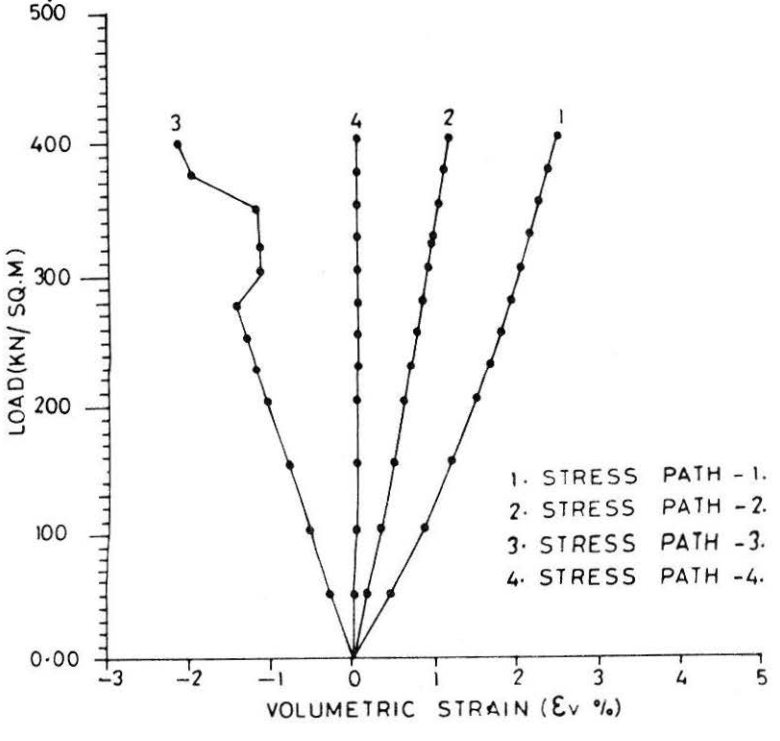

FIGURE 6(c) Load Vs. Volumetric Strain Behaviour For Paris Clay

dimensional Finite Element Method using eight noded isoparametric brick elements is used in the analysis. The results are presented in the form of load-deformation behavior for three types of soils.

The following conclusions are drawn based on the analysis.

1. The model suggested by Yin et al (1989) can easily be implemented to get the load-deformation behavior for the foundation resting on soil.

2. The load-deformation behavior obtained is non-linear from the beginning and a well defined yield point is indicated.

3. The change in volume of the elements obtained during loading indicates the heaving and the settlement of the foundation soil as observed by many investigators for the behavior of foundation resting on soil.

Thus the model is capable of predicting the realistic behavior of foundation on soil.

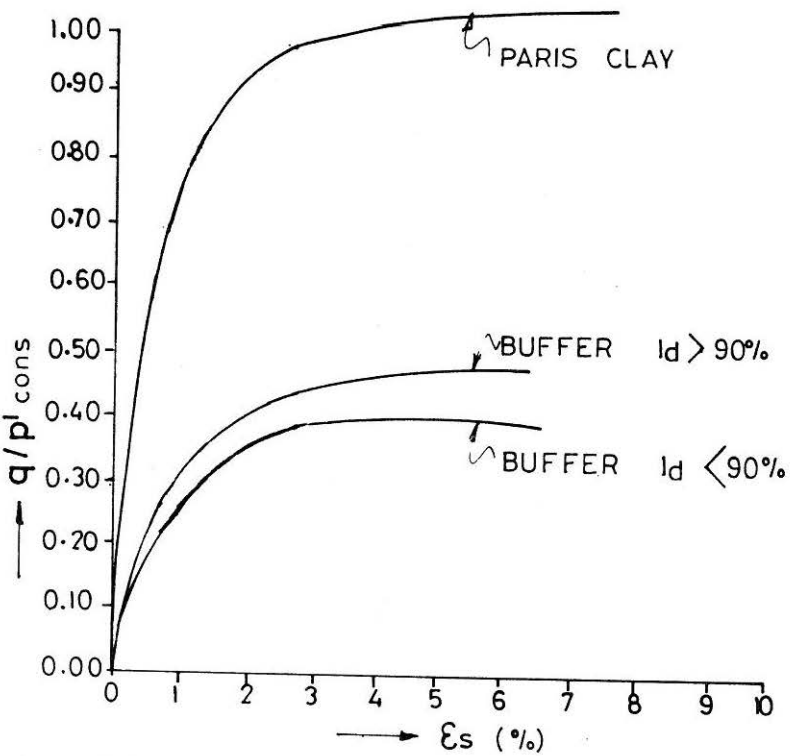

FIGURE 7 q/P'_{cons} Vs. ε_s Behaviour For Different Types Of Soils As Given By Yin et. al., (1989)

Aknowledgement

The author is indebted to Prof. U.D. Kamath, Head of Department, Civil Engineering, M. I. T., Manipal for the computer facilities provided to conduct this study.

References

ATKINSON, J.H. AND BRANSBY, P.L. (1978) : "The Mechanics of Soils." McGraw-Hill Book Company, U.K.

CHANDRAKANT S. DESAI AND JOHN F. ABEL (1972) : "Introduction to the Finite Element Method."Litton Educational Publishing Company, New Delhi.

KRISHNAMOORTHY, C.S. (1987) : "Finite Element Analysis. "Tata McGraw -Hill Publishing Company, New Delhi.

MADHIRA, R. MADHAV AND KARMARKAR, R.S. (1982) : "Elasto-Plastic settlement of rigid footings." ASCE, Vol. 108, No. GT3: pp 483-487.

RAO, N.B.S. (1981) : "Constitutive laws for soft clays." Proc.of the symposium on implementatian of computer procedures and stress-strain laws in geotechnical Engineering., New York, 1981.

TEKEJI KOKUSHO (1978) : "Nonlinear Analysis of a soil with arbitrary dilatancy by Finite Element Method." *Soils and Foundations*, Vol. 18, No.1.

YIN, J.H. (1989) : "Constitutive modelling of soil behavior using three modulus hypoelasticity." 12th International Conference SMFE, Volume 1, pp 143.

VARMEER, P.A. (1978) : "A double hardening model for sand." *Geotechnique*, Vol. 28, No. 4, pp 413-433.

ZINKIEWICZ, O.C. (1977) : "The Finite Element Method." McGraw Hill Book Company, U.K.

Appendix - 1

The increment of strains corresponding to the increments of stresses can be related as,

$$\begin{vmatrix} d\varepsilon_{11} \\ d\varepsilon_{22} \\ d\varepsilon_{33} \\ d\varepsilon_{12} \\ d\varepsilon_{23} \\ d\varepsilon_{31} \end{vmatrix} = \begin{vmatrix} a_1 + 2b_1 & a_2 + b_1 + b_2 & a_2 + b_1 + b_3 & c_1 & c_2 & c_3 \\ a_2 + b_1 + b_2 & a_1 + 2b_2 & a_2 + b_2 + b_3 & c_1 & c_2 & c_3 \\ a_2 + b_1 + b_3 & a_2 + b_2 + b_3 & a_1 + 2b_3 & c_1 & c_2 & c_3 \\ \frac{c_1}{2} & \frac{c_2}{2} & \frac{c_3}{2} & \frac{1}{2G} & 0 & 0 \\ \frac{c_1}{2} & \frac{c_2}{2} & \frac{c_3}{2} & 0 & \frac{1}{2G} & 0 \\ \frac{c_1}{2} & \frac{c_2}{2} & \frac{c_3}{2} & 0 & 0 & \frac{1}{2G} \end{vmatrix} \begin{vmatrix} d\sigma_{11} \\ d\sigma_{22} \\ d\sigma_{33} \\ d\sigma_{12} \\ d\sigma_{23} \\ d\sigma_{31} \end{vmatrix} \quad \ldots\ldots \text{(i)}$$

where,

$$a1 = 1/9k + 1/3G$$
$$a2 = 1/9k - 1/6G$$
$$b1 = \{2(\sigma 1) - \sigma 2 - \sigma 3\}/6\,q\,J$$
$$b2 = \{2(\sigma 2) - \sigma 1 - \sigma 3\}/6\,q\,J$$
$$b3 = \{2(\sigma 3) - \sigma 1 - \sigma 2\}/6\,q\,J$$
$$c1 = \sigma 12/q\,J$$
$$c2 = \sigma 23/q\,J$$
$$c3 = \sigma 31/q\,J$$

Also

$$K = P'/\lambda/V_i \qquad \text{(ii)}$$

$$J = K\,n\,A^{1/n}(q/P'_{cons})^{n-1/n} \qquad \text{(iii)}$$

$$G = D\,J^2/(J^2 + 3DK) \qquad \text{(iv)}$$

$$D = \frac{1}{3} E \exp\{(\varepsilon_v - \varepsilon_{vo})V_i/\lambda\}\left[1 - F\,q \exp\{-(\varepsilon_v - \varepsilon_{vo})V_i/\lambda\}\right] \qquad \text{(v)}$$

$$\varepsilon_v = \lambda/V_i \ln(P'_{cons}) + \varepsilon_{vo}$$

Isotropic consolidation test provides data that relates effective mean stress p′ and volumetric strain ε_v. Fitting appropriate functions to these data leads to the equation,

$$\varepsilon_v = \lambda/V_i \ln(P'_{cons}) + \varepsilon_{vo}$$

where $V_i = 1 + eo$, the initial specific volume before loading. λ/V_i and ε_{vo} can be calculated by fitting appropriate curve. The values of K for any stress level corresponding to p′ can then be obtained from equation (ii) .

Consolidated undrained test ($\varepsilon_{vo} = 0$) gives two independent relationships between p'/P'_{cons} vs q/P'_{cons} and q/P'_{cons} vs ε_s. The first of this is used to calculate the values of A and n by using the equation,

$$q/P'_{cons} = A\left(1 - P'/P'_{cons}\right)^n$$

The value of J can then be obtained by using the equation-(iii).

The second relationship between ε_s vs $\varepsilon_s/q/P'_{cons}$ is used to determine the values of E and F by using the equation

$$q/P'_{cons} = \varepsilon_s/(E + F\varepsilon_s)$$

The value of D can then be obtained from equation (v). The value of G is then calculated by using the equation (iv).